

Many-body approach to infinite non-periodic systems: application to the surface of semi-infinite jellium

G. Fratesi* and G. P. Brivio†

*INFM and Dipartimento di Scienza dei Materiali,
Università di Milano-Bicocca, via Cozzi 53, I-20125 Milano*

L. G. Molinari

*Dipartimento di Fisica dell'Università degli Studi di Milano
Via Celoria 16, I-20133 Milano‡*

(Dated: November 20, 2018)

A method to implement the many-body Green function formalism in the GW approximation for infinite non periodic systems is presented. It is suitable to treat systems of known “asymptotic” properties which enter as boundary conditions, while the effects of the lower symmetry are restricted to regions of finite volume. For example, it can be applied to surfaces or localized impurities. We illustrate the method with a study of the surface of semi-infinite jellium. We report the dielectric function, the effective potential and the electronic self-energy discussing the effects produced by the screening and by the charge density profile near the surface.

PACS numbers: 71.10.-w, 73.20.-r

I. INTRODUCTION

Density functional theory (DFT) is central to the understanding of several fundamental problems in condensed matter physics, since it allows for obtaining the ground state properties of the system in a very accurate and computationally feasible way within an *ab initio* framework. However, current approximations of the exchange correlation functional are based mainly on the Local Density Approximation (LDA), and hence on the properties of the homogeneous electron gas. Therefore they cannot account correctly for fundamental physical phenomena, like weak bonding, and consequently the van der Waals interaction. At surfaces, the LDA and derived Generalized Gradient Approximation (GGA) functionals are unsatisfactory and corrections for surface specific errors were recently proposed.¹ Another example of the failure of the LDA/GGA is the potential calculated at large distances from a metal surface, which instead of reproducing the classical image one,² displays an exponential decay. This because the LDA/GGA neglects the long range electron correlations due to the inhomogeneity of the surface charge density.

A way to improve on the limitations of the DFT solution caused by approximated exchange-correlation functionals is to resort to methods of many-body perturbation theory. This also gives access to physical properties outside the realm of DFT, such as quasiparticle and collective excitations.

The many-body problem was expressed by Hedin³ as a formally exact closed set of five equations that relate the single particle Green’s function, the self-energy, the polarization, the effective two-particle potential and the vertex function. The GW approximation^{4,5} (GWA) neglects vertex corrections and reduces Hedin’s system to four closed equations. The results of DFT can be used to achieve an efficient scheme of solution of the GW equa-

tions. In fact Dyson’s equation for the exact Green function requires the input of a reference one, which in the original Hedin’s formulation is the Green function for the Hartree equation. A great improvement is to use instead the Green function of the Kohn-Sham (KS) equation, since it includes not only the Hartree potential but also exchange and correlation effects to some local degree of correctness. This minimizes the effort for self-consistency in the evaluation of the density.

The GWA with the just mentioned input from DFT is a strategy that has been successfully applied to several systems. It combines the efficiency of the KS equation, with the use of the basic equations of many body theory, and it is able to supply reliable ground state properties as well as excitation energies, lifetimes, and generalized dielectric functions. For example the surface effective potential $V_{XC}(z)$ with the correct image tail was achieved by Eguluz *et al.*,² by solving the Sham-Schlüter equation in GWA, with a slab geometry.

As already pointed out, DFT, sometimes coupled to the GWA especially for excited state properties,⁶ have allowed for a realistic and accurate treatment of more and more complex systems of condensed matter physics. Among them, a single bulk impurity, solid surfaces, adsorbed molecules and clusters, interfaces as well as the recently investigated nano-contacts are indeed infinite or semi-infinite non-periodic electronic systems. However, in the theoretical description, such systems are usually confined in a ficticiously finite region/supercell with periodic properties at the boundaries.⁷ Consequently artificial features may occur: for example, spurious interactions, non-physical oscillatory behaviors of the wavefunctions, and a discrete spectrum in which it may be difficult to isolate localized electronic states and resolve resonant ones. For example, in order to properly account for the underlying bulk band structure, a DFT evaluation of the surface dielectric function for a semi-infinite crys-

tal, that avoids slab or supercell geometries, was recently proposed by Brodersen and Schattke.⁸

In this paper we address the problem of the description of an infinite non-periodic system within a GWA framework. We show here that the artificial reduction of an infinite volume to a periodic one can be avoided with minimal computational cost and more transparent results. Our method applies to systems (like surfaces or localized impurities) that asymptotically in space identify with others whose relevant correlators are well studied, like bulk crystal or vacuum. It relies on the assumption that, for any relevant correlator $F(1, 2)$, there is a *finite* space region U_F outside which $F(1, 2)$ cannot be distinguished from its asymptotic limit $F^\infty(1, 2)$, within the required accuracy. This property is under control in the course of computation. It also provides a powerful tool for checking the correctness of the result, by verifying whether the correlator F matches with F^∞ at the boundaries of U_F or not.

The virtue of this method is to *replace the finite volume of the cell or slab by a finite effective volume U_F with boundary conditions that are intrinsic to the system.* The property that “asymptotic” regions actually determine an effective region U_F of finite volume for the computation is connected with the principle of *nearsightedness* recently introduced by Kohn.^{9,10} It states that the local electronic structure near a point \mathbf{r} , while requiring in principle the knowledge of the density (or the effective potential) everywhere, is largely determined by the potential near \mathbf{r} .

In Sec. II we shall present the main points of the GWA to set the stage for further developments. Sec. III outlines the method. Two main ingredients are the embedding approach for the zero-th order Green function, which guarantees that the properties of the infinite non-periodic system are taken correctly into account, and a Lemma for the inversion of infinite matrices. The application to the semi-infinite jellium is worked out in Sec. IV. Because of its generality, the jellium surface is currently used as a bench mark system to evaluate many-body features.¹¹ The extension of the GWA to the semi-infinite jellium can provide further data especially on how many-body properties affect the spectral ones by calculating the dielectric function, the effective potential and the self-energy for a true continuum. Finally Sec. V is devoted to the conclusions.

II. THE GW APPROXIMATION

We wish to carry out a many-body treatment of an infinite non periodic system in the GWA. In order to present our work in a self-contained way, in this section we recall the basic properties and the equations of the GWA. To be specific, we write the Hamiltonian of a system of electrons with Coulomb interaction $v(\mathbf{r}, \mathbf{r}')$, in a static external potential $V_{\text{ext}}(\mathbf{r})$ that couples to the den-

sity $\hat{n}(\mathbf{r})$:

$$\hat{H} = \sum_i \frac{1}{2} \hat{\mathbf{p}}_i^2 + \sum_{i < j} v(\hat{\mathbf{r}}_i, \hat{\mathbf{r}}_j) + \int d\mathbf{r} V_{\text{ext}}(\mathbf{r}) \hat{n}(\mathbf{r}). \quad (1)$$

Atomic units ($a_0 = 0.529 \text{ \AA}$, 1 hartree = 27.2 eV) are used throughout this paper. Since we are not interested in a spin-polarized phase, we consider a ground state with equal occupations for spin. The fermionic correlators are then proportional to the unit spin matrix. Two-point correlators, $F(1, 2) \equiv F(\mathbf{r}_1 t_1, \mathbf{r}_2 t_2)$ are time translation invariant and will be considered in frequency space:

$$F(\mathbf{r}_1 t_1, \mathbf{r}_2 t_2) = \int_{-\infty}^{+\infty} \frac{d\omega}{2\pi} F(\mathbf{r}_1, \mathbf{r}_2, \omega) e^{-i\omega(t_1 - t_2)}. \quad (2)$$

The GWA^{4,5} is a self-consistent scheme that originates from truncating the exact closed set of five Hedin’s equations for the five basic quantities: Green function G , self-energy Σ , effective potential W , polarization P , and vertex function Γ . In the GWA the first two Hedin’s equations, namely the Dyson equations for the Green function G and for the effective potential W , remain the same.

The computational effort is reduced if, in the Dyson equation for G , one makes reference to the Green function G_0 that solves the KS equation:

$$\left[\omega + \frac{1}{2} \nabla_{\mathbf{r}}^2 - V_{\text{KS}}(\mathbf{r}) \right] G_0(\mathbf{r}, \mathbf{r}', \omega) = \delta(\mathbf{r} - \mathbf{r}'), \quad (3)$$

$$V_{\text{KS}}(\mathbf{r}) = V_{\text{H}}(\mathbf{r}) + V_{\text{ext}}(\mathbf{r}) + V_{\text{XC}}(\mathbf{r}). \quad (4)$$

The Hartree potential $V_{\text{H}}(\mathbf{r}) = \int d\mathbf{r}' v(\mathbf{r}, \mathbf{r}') n(\mathbf{r}')$ and the exchange-correlation potential $V_{\text{XC}}(\mathbf{r})$ contain the unknown density of the interacting system, which is to be found self-consistently by the relation $n(\mathbf{r}) = -2i \int d\omega G_0(\mathbf{r}, \mathbf{r}, \omega) e^{i\omega\eta}$. The factor $e^{i\omega\eta}$, where $\eta \rightarrow 0^+$, results from time-ordering of operators and ensures appropriate analytic properties.

It is simple to check that the exchange-correlation potential in Eq. (4) modifies the Dyson equation for the Green function into:

$$G(\mathbf{r}_1, \mathbf{r}_2, \omega) = G_0(\mathbf{r}_1, \mathbf{r}_2, \omega) + \int d\mathbf{r}_3 \int d\mathbf{r}_4 G_0(\mathbf{r}_1, \mathbf{r}_3, \omega) \times (\Sigma_{\text{XC}}(\mathbf{r}_3, \mathbf{r}_4, \omega) - V_{\text{XC}}(\mathbf{r}_3) \delta(\mathbf{r}_3 - \mathbf{r}_4)) G(\mathbf{r}_4, \mathbf{r}_2, \omega). \quad (5)$$

Since the Hartree potential is accounted for exactly in the KS Eq. (3), the self-energy diagrams are all of exchange-correlation type (with no tadpoles). The Dyson equation for the effective potential is:

$$W(\mathbf{r}_1, \mathbf{r}_2, \omega) = v(\mathbf{r}_1, \mathbf{r}_2) + \int d\mathbf{r}_3 \int d\mathbf{r}_4 v(\mathbf{r}_1, \mathbf{r}_3) P(\mathbf{r}_3, \mathbf{r}_4, \omega) W(\mathbf{r}_4, \mathbf{r}_2, \omega). \quad (6)$$

Next, there are the two Hedin’s equations that basically result from the unique skeleton diagrams¹² of the exchange-correlation self-energy and of the polarization.

In the GWA they simplify, as one identifies the vertex with the bare one.

$$\Sigma_{\text{XC}}(\mathbf{r}_1, \mathbf{r}_2, \omega) = i \int_{-\infty}^{+\infty} \frac{d\omega'}{2\pi} e^{i\omega'\eta} G(\mathbf{r}_1, \mathbf{r}_2, \omega + \omega') W(\mathbf{r}_2, \mathbf{r}_1, \omega'), \quad (7)$$

$$P(\mathbf{r}_1, \mathbf{r}_2, \omega) = -2i \int_{-\infty}^{+\infty} \frac{d\omega'}{2\pi} e^{i\omega'\eta} G(\mathbf{r}_1, \mathbf{r}_2, \omega + \omega') G(\mathbf{r}_2, \mathbf{r}_1, \omega'). \quad (8)$$

The fifth Hedin's equation is neglected in GWA and corresponds to the skeleton expansion of the vertex, which is made of an infinite number of diagrams. The inclusion of vertex corrections is computationally expensive and difficult, with a degree of arbitrariness.¹³

Finally we recall the following useful symmetry property of any correlator due to the invariance under time-reversal of the Hamiltonian:

$$F(\mathbf{r}_1, \mathbf{r}_2, \omega) = F(\mathbf{r}_2, \mathbf{r}_1, \omega) \quad (9)$$

For the polarization P and the effective potential W , Eq. (9) implies further that they are even functions of the frequency ω . Such exact properties are preserved by the GWA.

III. THE METHOD

In this section we present a method to evaluate the interacting Green function of Eq. (5) in the KS+GW scheme, for an infinite non-periodic system. In general in the GWA one has to perform the following operations: (i) Evaluation of the KS Green function G_0 in Eq. (3). (ii) Evaluation of the ring diagram for P_0 in Eq. (8). (iii) Evaluation of W_0 by solving the Dyson Eq. (6). (iv) Evaluation of $\Sigma_0 = iG_0W_0$ in Eq. (7). (v) Evaluation of G_1 by solving the Dyson Eq. (5).

In principle, one should iterate the cycle (ii-v) for self-consistency, by inserting G_1 in step (ii). Experience with the homogeneous electron gas (HEG) has shown that spectral properties are better reproduced by a first-iteration calculation rather than by a self-consistent one.¹⁴

For periodic systems, the calculations can be restricted to a finite volume (e.g., the unit cell of a lattice crystal) with suitable boundary conditions. The present method implements the same procedure for infinite systems in a viable way. A weaker hypothesis is used: along the directions of broken symmetry any correlator F can be approximated by the known F^∞ except for a finite length. Hence the calculation is carried on only in a finite volume, with boundary conditions determined by the "asymptotic properties of the system", i.e., by F^∞ . A direct space representation will be privileged in the directions where periodicity is absent.

A. Preliminary steps

We present two main ingredients which allow for the development of our method: the Green function embedding method to calculate G_0 in Eq. (3), and a Lemma for the inversion of infinite matrices, which permits to solve the Dyson equations for G_1 and W_0 in Eq. (5) and Eq. (6), respectively.

1. The embedding method

To start, the Green function G_0 of the KS equation (3) is needed. We make use of the Green function embedding method.^{15,16,17} Such a tool has been applied successfully to the study of infinite systems without 3D periodicity, such as bulk impurities, surfaces and adsorbates.⁷ Its great advantage compared to the slab and the supercell techniques is to provide a truly continuous density of states and the correct asymptotic behavior of all physical quantities close enough to the defect region. In the embedding method, space divides into a finite region V and one (or many) region V' where the asymptotic regime is valid to the required accuracy. In this approach, the KS equation (3) in $V \cup V'$ is rewritten as an equation for the finite region V only. The effect of V' appears as a surface term that adds to the KS potential. The modified KS equation, for \mathbf{r} and \mathbf{r}' in V reads as:

$$[\omega - H_{\text{KS}}(\mathbf{r})]G_0(\mathbf{r}, \mathbf{r}', \omega) - \int_S d^2\mathbf{r}'' U_S(\mathbf{r}, \mathbf{r}'', \omega) G_0(\mathbf{r}'', \mathbf{r}', \omega) = \delta(\mathbf{r} - \mathbf{r}'), \quad (10)$$

where $H_{\text{KS}} = -\frac{1}{2}\nabla_{\mathbf{r}}^2 + V_{\text{KS}}$ and S is the boundary of V . The kernel $U_S(\mathbf{r}, \mathbf{r}'', \omega)$ is non-zero only for $\mathbf{r}, \mathbf{r}'' \in S$, where it is:

$$U_S(\mathbf{r}, \mathbf{r}', \omega) = \frac{1}{2} \delta_S(\mathbf{r}, \mathbf{r}') \mathbf{n}_S(\mathbf{r}) \cdot \nabla_{\mathbf{r}} + (G_0^\infty)^{-1}(\mathbf{r}, \mathbf{r}', \omega) \quad (11)$$

$\mathbf{n}_S(\mathbf{r})$ is the unit vector normal to S in \mathbf{r} , pointing out of V . $G_0^\infty(\mathbf{r}, \mathbf{r}', \omega)$ is the Green function of the KS equation in the asymptotic region V' , with Neumann boundary condition on S :

$$[\omega - H_{\text{KS}}(\mathbf{r})]G_0^\infty(\mathbf{r}, \mathbf{r}', \omega) = \delta(\mathbf{r} - \mathbf{r}'), \quad (12)$$

$$\mathbf{n}_S(\mathbf{r}) \cdot \nabla_{\mathbf{r}} G_0^\infty(\mathbf{r}, \mathbf{r}', \omega) = 0. \quad (13)$$

$(G_0^\infty)^{-1}$ is the surface functional inverse of G_0^∞ , defined for points on S :

$$\int_S d^2\mathbf{r}' G_0^\infty(\mathbf{r}_1, \mathbf{r}', \omega) (G_0^\infty)^{-1}(\mathbf{r}', \mathbf{r}_2, \omega) = \delta_S(\mathbf{r}_1, \mathbf{r}_2). \quad (14)$$

Eq. (10) can be expanded over a countable basis of V , thus reducing the evaluation of G_0 to a matrix inversion, which can be equally done for real or complex frequencies. We emphasize that the embedding method is formally

exact so that G_0 exhibits the truly *continuous* spectrum of the system. Being the solution of Eq. (10), G_0 is known only for \mathbf{r} and \mathbf{r}' both in V . When the value of G_0 for one or both arguments outside V is required, it can be obtained with the “matching Green function” method.¹⁸

2. Inversion of infinite matrices

Consider the equations defining the inverse of a matrix A on two different volumes Ω and V , with $V \subset \Omega$:

$$\int_{\Omega} d\mathbf{r}_3 A(\mathbf{r}_1, \mathbf{r}_3) A_{\Omega}^{-1}(\mathbf{r}_3, \mathbf{r}_2) = \delta(\mathbf{r}_1 - \mathbf{r}_2), \quad \mathbf{r}_1, \mathbf{r}_2 \in \Omega, \quad (15)$$

$$\int_V d\mathbf{r}_3 A(\mathbf{r}_1, \mathbf{r}_3) A_V^{-1}(\mathbf{r}_3, \mathbf{r}_2) = \delta(\mathbf{r}_1 - \mathbf{r}_2), \quad \mathbf{r}_1, \mathbf{r}_2 \in V. \quad (16)$$

In general A_V^{-1} is different from the restriction of A_{Ω}^{-1} in V . However, the following Lemma gives a condition for the two matrices to coincide on a smaller subset $U \subset V \subset \Omega$.

Lemma: If $A_{\Omega}^{-1}(\mathbf{r}_1, \mathbf{r}_2) = 0$ for all $\mathbf{r}_1 \in \Omega - V$ and $\mathbf{r}_2 \in U$, then $A_{\Omega}^{-1}(\mathbf{r}_1, \mathbf{r}_2) = A_V^{-1}(\mathbf{r}_1, \mathbf{r}_2)$ for all $\mathbf{r}_1, \mathbf{r}_2 \in U$. Proof: consider Eq. (15) for $\mathbf{r}_1 \in V$ and $\mathbf{r}_2 \in U$, multiply it by $A_V^{-1}(\mathbf{r}_4, \mathbf{r}_1)$ and integrate in \mathbf{r}_1 over V :

$$\int_V d\mathbf{r}_1 A_V^{-1}(\mathbf{r}_4, \mathbf{r}_1) \int_{\Omega} d\mathbf{r}_3 A(\mathbf{r}_1, \mathbf{r}_3) A_{\Omega}^{-1}(\mathbf{r}_3, \mathbf{r}_2) = A_V^{-1}(\mathbf{r}_4, \mathbf{r}_2).$$

The integral in \mathbf{r}_3 over Ω is split into an integral on V and on $\Omega - V$. The first integral yields $A_{\Omega}^{-1}(\mathbf{r}_4, \mathbf{r}_2)$, the latter vanishes because $A_{\Omega}^{-1}(\mathbf{r}_1, \mathbf{r}_2) = 0$ for $\mathbf{r}_1 \in \Omega - V$ and $\mathbf{r}_2 \in U$. •

As a consequence of the Lemma, if we are interested in the values of A_{Ω}^{-1} in a subset U of the possibly infinite volume Ω , it is sufficient to invert A on a suitable *larger* subset V , with $V \subset \Omega$. Quite generally, the functions of interest have the property $A_{\Omega}^{-1}(\mathbf{r}_1, \mathbf{r}_2) \rightarrow 0$ as $|\mathbf{r}_1 - \mathbf{r}_2| \rightarrow \infty$. Therefore, the hypothesis of the Lemma can be regarded as true to any degree of accuracy, for a large enough set V .

B. Steps of the method

1. The polarization

In direct space and GWA, the polarization P_0 is given by the ring diagram [Eq. (8)] with Green functions G_0 .

To compute it numerically, we note that the convergence of the integration in Eq. (8) is improved by using $\Delta G_0 = G_0 - G_0^{\infty}$, which decays faster than G_0 as $|\omega| \rightarrow \infty$. Hence we can take advantage of the known function P_0^{∞} , that corresponds to the asymptotic limit of P_0 continued into the region of interest. We can write:

$$P_0(\omega) = \int d\omega' [G_0^{\infty} + \Delta G_0](\omega + \omega') \times [G_0^{\infty} + \Delta G_0](\omega'). \quad (17)$$

The integration of the term containing $(G_0^{\infty} G_0^{\infty})$ gives P_0^{∞} , the others have a faster decay for large $|\omega|$. Owing to the non-analytic behaviour of the Green function close to the real axis, it is convenient to compute Eq. 17 on the contour described in the Appendix. Since the spatial dependence is not involved in the computation of the polarization $P_0(\mathbf{r}_1, \mathbf{r}_2, \omega)$, such dependence amounts to that of G_0 in the same region.

2. The effective potential

The effective (dressed) potential is the solution of the Dyson equation, Eq. (6), and it is formally given by the integral:

$$W_0(\mathbf{r}_1, \mathbf{r}_2, \omega) = \int d\mathbf{r}_3 \varepsilon^{-1}(\mathbf{r}_1, \mathbf{r}_3, \omega) v(\mathbf{r}_3, \mathbf{r}_2). \quad (18)$$

where ε^{-1} is the functional inverse of the dielectric function ε :

$$\varepsilon(\mathbf{r}_1, \mathbf{r}_2, \omega) = \delta(\mathbf{r}_1 - \mathbf{r}_2) - \int d\mathbf{r}_3 v(\mathbf{r}_1, \mathbf{r}_3) P_0(\mathbf{r}_3, \mathbf{r}_2, \omega). \quad (19)$$

The decay properties of the polarization P_0 as $|\mathbf{r}_1 - \mathbf{r}_2| \rightarrow \infty$ imply that Eq. (19) can be evaluated numerically by introducing cutoffs for the integration variable \mathbf{r}_3 .

The inverse dielectric function is formally defined by:

$$\int d\mathbf{r}_3 \varepsilon(\mathbf{r}_1, \mathbf{r}_3, \omega) \varepsilon^{-1}(\mathbf{r}_3, \mathbf{r}_2, \omega) = \delta(\mathbf{r}_1 - \mathbf{r}_2). \quad (20)$$

The inversion of the matrix ε on an unbounded region is not a feasible numerical calculation. However, we only need evaluate ε^{-1} on a finite region U_{ε} outside which the asymptotic regime holds. Since in ordinary systems the effective interaction between electrons far apart decays to zero as the distance increases, Eq. (18) implies that also $\varepsilon^{-1}(\mathbf{r}_1, \mathbf{r}_2)$ goes to zero as $|\mathbf{r}_1 - \mathbf{r}_2| \rightarrow \infty$. So we can use the Lemma proven in Sec. III A 2 and restrict the integration in Eq. (20) to a finite region V_{ε} , $U_{\varepsilon} \subset V_{\varepsilon}$, still obtaining correct values of $\varepsilon^{-1}(\mathbf{r}_1, \mathbf{r}_2)$ for $\mathbf{r}_1, \mathbf{r}_2 \in U_{\varepsilon}$. An expansion over a discrete basis set is now possible, leading the problem to an ordinary matrix inversion. The size of the region V_{ε} is simply a numerical parameter, and convergence in the resulting ε^{-1} must be checked. With this purpose, a localized basis set [like $\phi_i(\mathbf{r}) = c\delta(\mathbf{r} - \mathbf{r}_i)$] is more convenient. In this case the matrix elements ε_{ij}^{-1} , being directly proportional to $\varepsilon^{-1}(\mathbf{r}_i, \mathbf{r}_j)$, do not change except for the normalization factor c , when the size of V_{ε} or the number of basis function changes. The effective potential can now be evaluated from Eq. (18). We only remark that the frequency argument ω is fixed, so that W_0 is computed for the same values of ω as those chosen for the polarization – ω purely imaginary as shown in the Appendix.

Finally we note that the assertion that $\varepsilon^{-1}(\mathbf{r}_1, \mathbf{r}_2) \rightarrow 0$ as $|\mathbf{r}_1 - \mathbf{r}_2| \rightarrow \infty$ before ε^{-1} is actually evaluated does

not pose conceptual difficulties: the decay to zero has in fact to be checked for the known function $(\varepsilon^\infty)^{-1}$.

3. The self-energy

It is customary to split the self-energy into the sum of the exchange $\Sigma_X = iGv$ and the correlation term $\Sigma_C = iG(W - v)$. The evaluation of the exchange term poses no problem:

$$\Sigma_X(\mathbf{r}_1, \mathbf{r}_2) = iv(\mathbf{r}_1, \mathbf{r}_2) \int_{-\infty}^{+\infty} \frac{d\omega}{2\pi} e^{i\omega\eta} G_0(\mathbf{r}_1, \mathbf{r}_2, \omega). \quad (21)$$

The frequency integration sums over the occupied KS states, and can be performed analytically if the spectrum is discrete. In our case, the spectrum is generally continuous [G_0 is the solution of Eq.(10)], and the sum is replaced by an integral to be performed numerically. A change of contour proves useful, together with the information that we shall be dealing with systems in which there are no KS states below the bottom of the band E_0 (η' is a positive infinitesimal):

$$\begin{aligned} & \int_{-\infty}^{+\infty} d\omega e^{i\omega\eta} G_0(\omega) \\ &= \int_{E_0}^{\mu} d\omega [G_0(\omega - i\eta') - G_0(\omega + i\eta')]. \quad (22) \end{aligned}$$

The resulting integral is computed straightforwardly. μ is the KS chemical potential.

The correlation term is:

$$\Sigma_C(\omega) = i \int_{-\infty}^{+\infty} d\omega' e^{i\omega'\eta} G_0(\omega + \omega') [W_0(\omega') - v]. \quad (23)$$

Since the main contribution to the above integral is Σ_C^∞ , one can use the same splitting of the self-energy in Eq. (23) into a leading asymptotic term plus a correction due to the inhomogeneity as in Sec. III B 1 for the polarization.

Mathematical details on the calculation of the integrals determining the the self-energy are discussed in the Appendix.

4. The Green function

The Dyson equation for G [Eq. (5)] is formally the same as the Dyson equation for W [Eq. (6)] once G , $\Sigma_{XC} - V_{XC}$ and G_0 are identified with W , P , and v respectively. Therefore we define the function $\epsilon_{XC}(\mathbf{r}_1, \mathbf{r}_2, \omega)$, which is analogous to the dielectric function:

$$\begin{aligned} \epsilon_{XC}(\mathbf{r}_1, \mathbf{r}_2, \omega) &= \delta(\mathbf{r}_1 - \mathbf{r}_2) - \int d\mathbf{r}_3 G_0(\mathbf{r}_1, \mathbf{r}_3, \omega) \\ &\times [\Sigma_{XC}(\mathbf{r}_3, \mathbf{r}_2, \omega) - V_{XC}(\mathbf{r}_2)\delta(\mathbf{r}_3 - \mathbf{r}_2)]. \quad (24) \end{aligned}$$

Even with the these strong analogies, ϵ_{XC} presents a striking difference with ε : the decay of $\epsilon_{XC}(\mathbf{r}_1, \mathbf{r}_2)$ as $|\mathbf{r}_1, \mathbf{r}_2|$ goes to infinity is linked to the one of G_0 , which in turn varies according to the dimensionality of the system. As a consequence, $\epsilon_{XC}(\mathbf{r}_1, \mathbf{r}_2)$ may not go to zero as $|\mathbf{r}_1 - \mathbf{r}_2|$ goes to infinity, thus not satisfying the hypothesis of the Lemma in Sec. III A 2. To make G_0 decay as $|\mathbf{r} - \mathbf{r}'| \rightarrow \infty$ (which implies the same property for ϵ_{XC}), it is convenient to solve Eq. (24) at a complex frequency $\omega + i\Delta$. The choice of the real quantity Δ depends on a compromise: if it is too small, the decay of G_0 is very slow and a large region of inversion of ϵ_{XC} is needed; if it is too large, the structures on the real frequency axis we are interested in are broadened – in fact Δ plays the role of resolution. The final result of the calculation, the interacting Green function, is thus evaluated on a translated frequency axis $\omega + i\Delta$. Analytical continuation improves the resolution: first, the values of G are fitted with a rational function, then the expression is continued to the real frequency axis.

IV. SEMI-INFINITE JELLIUM

In this section we illustrate the application of the method to semi-infinite jellium.¹⁹

A. Introduction to the system

Semi-infinite jellium is a neutral system of dynamical electrons in a background of uniform positive charge density in the half-space $z \leq 0$. In the half-space $z > 0$ there is no positive charge. We denote the uniform density by n , $n = 1/(4\pi r_s^3/3)$. In the computations the value of r_s will be fixed to give an electron density equal to that of aluminium ($r_s = 2.07 a_0$).

Besides time translations and time reversal, the system is also invariant under translations parallel to the surface. Hence the wave-vector parallel to the surface \mathbf{k}_\parallel is a good quantum number. It is important to observe that since the solid is semi-infinite, the wave-vector k_z may take any real value. So we shall deal with truly continuous densities of states, also for a fixed \mathbf{k}_\parallel . A slab calculation would instead determine a discrete spectrum (i.e., a nonphysical quantized set of k_z wave-vectors). Because of the just mentioned symmetry, a two-point correlator $F(\mathbf{r}_\parallel, z; \mathbf{r}'_\parallel, z'; \omega)$ only depends on the difference $\mathbf{r}_\parallel - \mathbf{r}'_\parallel$, where $\mathbf{r}_\parallel = (x, y)$. We can express F in terms of its Fourier transform (FT) with respect to a wave vector parallel to the surface:

$$F(\mathbf{r}_\parallel, z; \mathbf{r}'_\parallel, z'; \omega) = \int \frac{d\mathbf{k}_\parallel}{(2\pi)^2} e^{i\mathbf{k}_\parallel \cdot (\mathbf{r}_\parallel - \mathbf{r}'_\parallel)} F(z, z', \mathbf{k}_\parallel, \omega). \quad (25)$$

Since the system is also invariant under rotations around the z -axis, F depends only on the modulus of \mathbf{k}_\parallel .

The study of semi-infinite jellium is basically one-dimensional and satisfies the requirements of applicability of our method. In fact, the perturbation induced by the jellium edge is localized near the surface. At a distance of few r_s inside the solid, the properties of the system approach those of the infinite, homogeneous electron gas (HEG). Many-body results for the HEG in the GW approximation are well known in the literature.¹⁴ If we indicate by $F_n^{\text{HEG}}(k, \omega)$ the correlator F evaluated for a HEG of density n , the bulk and vacuum limits of F are

$$F_{\text{B,V}}^\infty(z, z', k_\parallel, \omega) = \int \frac{dk_z}{2\pi} e^{ik_z(z-z')} F_{n,0}^{\text{HEG}}(\sqrt{\mathbf{k}_\parallel^2 + k_z^2}, \omega) \quad (26)$$

Therefore we need evaluate the correlator F only on a limited interval $[z_{\text{B}}, z_{\text{V}}]$ of the z -axis, which will be the volume U_F of the previous Sec. III A 2.

Care must be taken when F is evaluated at z and z' in different regions of space, e.g., z in bulk and z' in vacuum. However, we are working with functions with the important property $F(z, z') \rightarrow 0$ when $|z - z'| \rightarrow \infty$.

This guarantees that when z is in bulk and z' in vacuum the functions $F_{\text{B}}(z, z')$ and $F_{\text{V}}(z, z')$ are both zero to the desired accuracy, provided that $|z_{\text{B}} - z_{\text{V}}|$ is large enough.

The dependence of F on its four arguments $(z, z', k_\parallel, \omega)$ is in principle continuous. Numerically, we stored the information about F on a four dimensional discrete mesh. Intermediate values, when necessary, are obtained with interpolation algorithms. For z and z' meshes, natural limit values are given by z_{B} and z_{V} . Cutoffs for k_\parallel and ω can be fixed since $F \rightarrow 0$ when $k_\parallel \rightarrow \infty$ or $|\omega| \rightarrow \infty$. Different meshes have to be chosen for different functions. Numerical convergence must be checked for any parameter defining the mesh.

B. G_0W_0 equations

In the chosen representation, the G_0W_0 equations (5-8) take the form:

$$P_0(z_1, z_2, k_\parallel, \omega) = -2i \int_{-\infty}^{+\infty} \frac{d\omega'}{2\pi} \int \frac{d^2\mathbf{k}'_\parallel}{(2\pi)^2} e^{i\omega'\eta} G_0(z_1, z_2, |\mathbf{k}_\parallel + \mathbf{k}'_\parallel|, \omega + \omega') G_0(z_2, z_1, k'_\parallel, \omega'), \quad (27a)$$

$$W_0(z_1, z_2, k_\parallel, \omega) = v(|z_1 - z_2|, k_\parallel) + \int dz_3 \int dz_4 v(|z_1 - z_3|, k_\parallel) P_0(z_3, z_4, k_\parallel, \omega) W_0(z_4, z_2, k_\parallel, \omega), \quad (27b)$$

$$\Sigma_{\text{XC}}(z_1, z_2, k_\parallel, \omega) = i \int_{-\infty}^{+\infty} \frac{d\omega'}{2\pi} \int \frac{d^2\mathbf{k}'_\parallel}{(2\pi)^2} e^{i\omega'\eta} G_0(z_1, z_2, |\mathbf{k}_\parallel + \mathbf{k}'_\parallel|, \omega + \omega') W_0(z_2, z_1, k'_\parallel, \omega'), \quad (27c)$$

$$G_1(z_1, z_2, k_\parallel, \omega) = G_0(z_1, z_2, k_\parallel, \omega) + \int dz_3 \int dz_4 G_0(z_1, z_3, k_\parallel, \omega) \times (\Sigma_{\text{XC}}(z_3, z_4, k_\parallel, \omega) - V_{\text{XC}}(z_3) \delta(z_3 - z_4)) G_1(z_4, z_2, k_\parallel, \omega), \quad (27d)$$

where v is the FT of Coulomb's potential:

$$v(|z_1 - z_2|, k_\parallel) = \frac{2\pi}{k_\parallel} e^{-k_\parallel |z_1 - z_2|}. \quad (28)$$

C. Steps of the calculation and results

We omit details regarding the starting point: the KS Green function $G_0(z, z', k_\parallel, \omega)$ can be obtained straightforwardly, with the embedding method described in Sec. III A 1. We calculated it in the LDA.

1. The polarization

The parallel-wavector convolution in Eq. (27a) does not pose numerical difficulties. Regarding the frequency convolution, the factor $e^{i\omega'\eta}$ is necessary for the convergence of the integral. In fact, the Green function $G_0(\omega)$ approaches zero like $|\omega|^{-1/2}$ as $|\omega| \rightarrow \infty$ (this can be easily verified for the HEG Green function). We follow the treatment of Sec. III B 1, and separate the integrand in two terms: one ($G_n^{\text{HEG}} G_n^{\text{HEG}}$), that gives P_n^{HEG} , and ($G_0 G_0 - G_n^{\text{HEG}} G_n^{\text{HEG}}$) that can be evaluated numerically, because it goes to zero as $|\omega|^{-3/2}$ when $|\omega| \rightarrow \infty$.

2. The effective potential

As shown in Sec. III B 2, one has to evaluate the dielectric function ϵ , defined by

$$\epsilon(z_1, z_2, k_{\parallel}, \omega) = \delta(z_1 - z_2) - \int dz_3 v(|z_1 - z_3|, k_{\parallel}) P_0(z_3, z_2, k_{\parallel}, \omega), \quad (29)$$

and its inverse ϵ^{-1} in order to solve Dyson equation for W , Eq. (27b):

$$W_0(z_1, z_2, k_{\parallel}, \omega) = \int dz_3 \epsilon^{-1}(z_1, z_3, k_{\parallel}, \omega) v(|z_3 - z_2|, k_{\parallel}). \quad (30)$$

The z integrations may be restricted to finite intervals since $P_0(z_1, z_2)$ and $\epsilon^{-1}(z_1, z_2)$ go to 0 as $|z_1 - z_2| \rightarrow \infty$. We also point out that the calculation time required by the integrals in Eqs. (29) and (30) is negligible, so the cutoffs of z can be cautiously overestimated.

To obtain ϵ^{-1} , defined by the inversion over the whole z -axis,

$$\int_{-\infty}^{+\infty} dz_3 \epsilon^{-1}(z_1, z_3) \epsilon(z_3, z_2) = \delta(z_1 - z_2), \quad (31)$$

on the finite interval $U_{\epsilon} = [z_B, z_V]$, we exploit the Lemma in Sec. III A 2 and restrict the integration in Eq. (31) to the finite interval $V_{\epsilon} = [L_B, L_V]$, $U_{\epsilon} \subset V_{\epsilon}$.

Correct values of $\epsilon^{-1}(z_1, z_2)$ for $z_1, z_2 \in U_{\epsilon}$ are obtained if L_B and L_V are conveniently large. It is sufficient that $\epsilon^{-1}(z, z_B) \simeq 0$ if $z < L_B$ and $\epsilon^{-1}(z, z_V) \simeq 0$ if $z > L_V$ to the required degree of accuracy. This concept is graphically presented in Fig. 1, where we show ϵ^{-1} for different values of L_B and L_V . The negative peak for $z_1, z_2 = L_B$ (on the left of each plot) represents a spurious feature introduced when the region of integration is restricted to a finite interval. Notice that this behavior is located at the boundaries of V_{ϵ} regardless to its size. Since $\epsilon^{-1}(z_1, z_2)$ is different from zero only for values of z_2 close to z_1 , this nonphysical feature is confined within few atomic units from the boundaries. Hence the interval V_{ϵ} has to be only slightly larger than U_{ϵ} . For the values described in Fig. 1, if $z_B = -15 a_0$, the choice $L_B = -20 a_0$ is already an accurate one. A similar discussion has to be done with respect to L_V , but in this case the spurious peak is much smaller.

In Fig. 2 we show the contour levels of the difference between the effective and bare interaction $W_0 - v$ in the z_1, z_2 plane. The HEG levels of the same quantity are also reported. The agreement is excellent when z_1 and z_2 approach bulk. As we move into the vacuum, $W_0 - v$ correctly goes to zero.

Next we consider the effective potential W_0 in the more intuitive representation, $(\mathbf{r}_1, \mathbf{r}_2, \omega)$, obtained by anti-FT with respect to \mathbf{k}_{\parallel} . For simplicity, we limit our discussion to the static case ($\omega = 0$) and consider collinear points

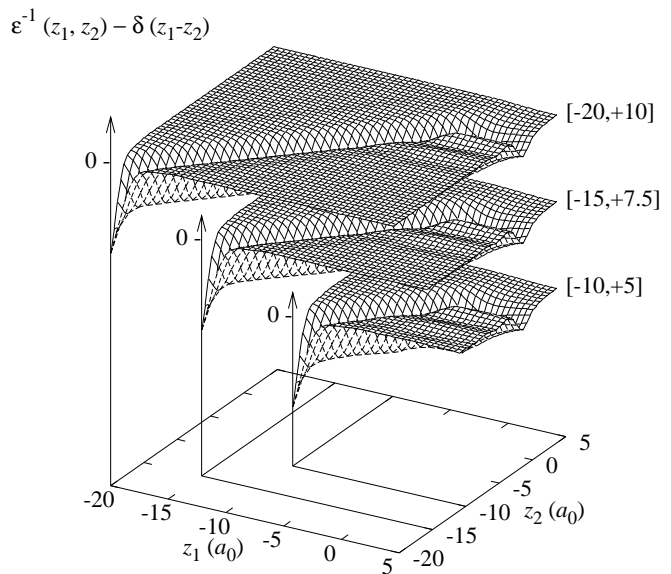


FIG. 1: Values of $\epsilon^{-1}(z_1, z_2) - \delta(z_1 - z_2)$ for different inverting regions $V_{\epsilon} = [L_B, L_V]$. Here, $r_s = 2.07 a_0$, $\omega = 0$ and $k_{\parallel} = 0.2k_F$, k_F being the Fermi wave-vector.

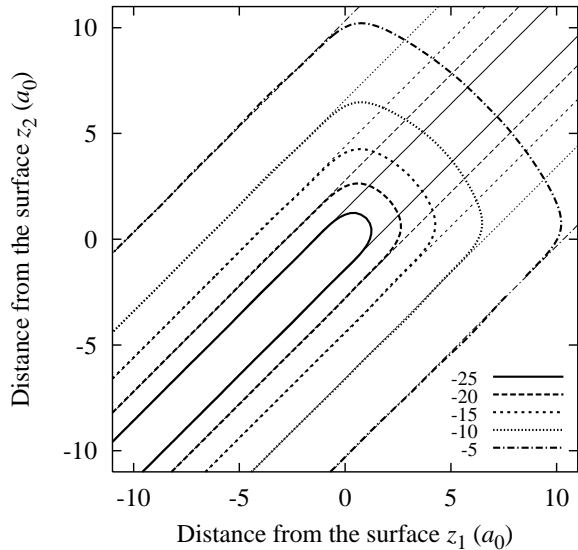


FIG. 2: Contour levels of $W_0(z_1, z_2, k_{\parallel}, \omega) - v(|z_1 - z_2|, k_{\parallel})$ in the z_1, z_2 plane. Thick curves: semi-infinite jellium. Thin curves: HEG of equal density. Here $r_s = 2.07 a_0$, $\omega = 0$ and $k_{\parallel} = 0.2k_F$.

on the normal to the surface ($\mathbf{r}_{1\parallel} = \mathbf{r}_{2\parallel}$). Fig. 3 shows the effective potential as a function of z from bulk to vacuum: W_0 is similar to a Yukawa screened potential for z_1 and z_2 in bulk, and it coincides with the bare Coulomb interaction for z_1 and z_2 in vacuum. Some intermediate values are shown: for z_1 fixed near the surface, W_0 is no longer a symmetric function of z_2 with respect to z_1 ,

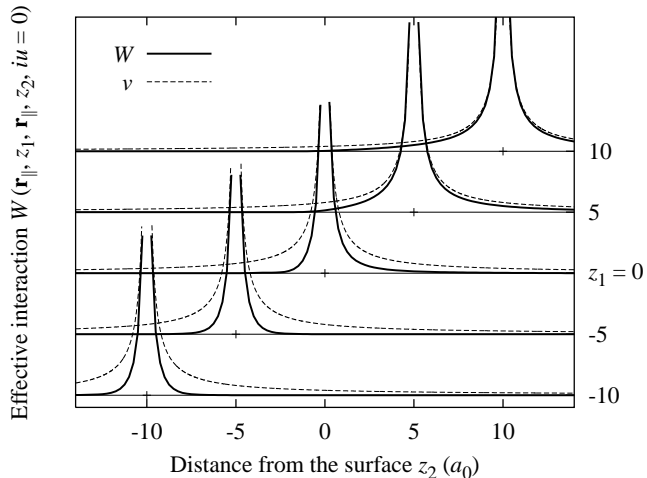


FIG. 3: Effective and bare Coulomb interactions near the jellium surface for points aligned on the normal. $r_s = 2.07 a_0$.

being the screening inhomogeneous.

3. The self-energy

The evaluation of the self-energy follows closely that of the polarization. However, differently from the previous case, it is not necessary to split the self-energy Σ_C into a leading term and a correction to it, as discussed in Sec. III B 3, because the difference $W - v$ decays fast enough to ensure convergence.

In Fig. 4 we report the contour levels of the self-energy evaluated at $k_{\parallel} = 0$ and $\omega = \mu$. Fig. 4(a) shows the result of our calculation: a particular feature in the near-surface region is the “arabian” shape of the contours levels. This arises because when z_1 and z_2 lie outside jellium, the self-energy, as $|z_1 - z_2|$ increases, decreases in a slower way than in bulk owing to lower screening.

In order to reduce the numerical effort required by a GW calculation, attempts have been made to mimic the self-energy with efficient models. In Fig. 4(b) we report the self-energy of a model based on fitting the spatial dependence of Σ from that of the HEG having the average density of the system, successfully tested for bulk silicon.²⁰ The surface peculiar contours in Fig. 4(a) cannot be reproduced by this model and the decay of Σ in vacuum is much slower. The comparison between these two results points out that a model based on an average density cannot reproduce features which are characteristic of a surface.

In Fig. 4(c) we show the self-energy evaluated from a G_0W_0 calculation where, instead of the self-consistent DFT-LDA Green function G_0 , one uses the Green function G_0^{step} computed for the approximated effective potential: $v_{\text{eff}}^{\text{step}}(z) = v_{\text{XC}}(-\infty)$ if $z \leq 0$ and $v_{\text{eff}}^{\text{step}}(z) = 0$ otherwise. It is well known that in this case there are stronger Friedel’s oscillations, and the electronic states

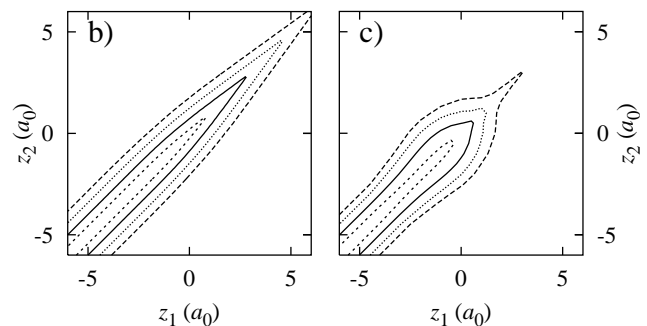
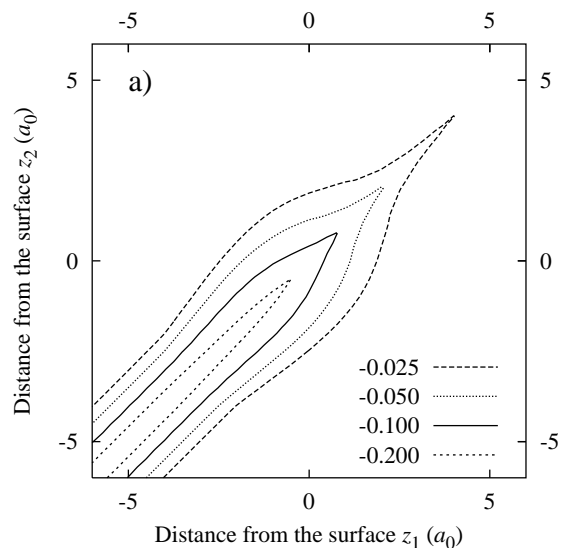


FIG. 4: Self-energy $\Sigma_{\text{XC}}(z_1, z_2, k_{\parallel}, \omega)$ for $r_s = 2.07 a_0$, $k_{\parallel} = 0$ and $\omega = \mu$. (a) Result of the GW computation. (b) Paula Sánchez-Friera’s model. (c) Step-potential approximation. Contour levels as in (a).

(and thus the Green function) decay faster away from the surface. This is reflected in the self-energy. Finally we remark that the difference between G_0W_0 and $G_0^{\text{step}}W_0^{\text{step}}$ is due primarily to the difference between the Green functions, whereas the effective interactions are very similar.

4. The interacting Green function

Following Eq. (24), the interacting Green function G_1 for the semi-infinite jellium can be evaluated from

$$G_1(z_1, z_2, k_{\parallel}, \omega) = \int dz_3 \epsilon_{\text{XC}}^{-1}(z_1, z_3, k_{\parallel}, \omega) G_0(z_3, z_2, k_{\parallel}, \omega), \quad (32)$$

where the kernel $\epsilon_{\text{XC}}^{-1}$ is obtained by inverting

$$\epsilon_{\text{XC}}(z_1, z_2, k_{\parallel}, \omega) = \delta(z_1 - z_2) - \int dz_3 G_0(z_1, z_3, k_{\parallel}, \omega) \times [\Sigma_{\text{XC}}(z_3, z_2, k_{\parallel}, \omega) - V_{\text{XC}}(z_2)\delta(z_3 - z_2)]. \quad (33)$$

When the frequency is infinitesimally close to the real axis and its real part corresponds to extended states, $G_0(z_1, z_3, k_{\parallel}, \omega)$, as a function of z_3 , is a plane wave with undamped oscillations propagating to infinity. As a consequence $\epsilon_{XC}^{-1}(z_1, z_2)$ does not go to zero as $|z_1 - z_2|$ goes to infinity, thus not satisfying the hypothesis of the Lemma. One must then recur to the procedure outlined in Sec. III B 4, i.e., solve Eq. (27d) at a complex frequency $\omega + i\Delta$. We experienced that an interval V_ϵ about $100 a_0$ wide was needed for a value of Δ of about 0.05 hartree, in order to describe the surface region correctly.

The imaginary part of the interacting Green function G yields the many-body spectral weight function

$$A(z, \mathbf{k}_{\parallel}, \omega) = -\frac{1}{\pi} \Im G(z, z, \mathbf{k}_{\parallel}, \omega) \text{sgn}(\omega - \mu). \quad (34)$$

This quantity gives a measure of the quasi-particle amplitude and is directly related to a variety of experiments such as photoemission spectroscopies,²¹ and scanning tunneling microscopy.²² The integral in \mathbf{k}_{\parallel} gives the local density of states (LDOS)

$$\sigma(z, \omega) = \int \frac{d^2 \mathbf{k}_{\parallel}}{(2\pi)^2} A(z, \mathbf{k}_{\parallel}, \omega). \quad (35)$$

The evaluation of the LDOS of semi-infinite jellium in this framework demonstrates the presence at the surface of a broad image-potential induced (IPI) resonance, which emerges sharply when results are compared to DFT-LDA ones. We stress that an IPI resonance width can only be obtained by a many-body approach like ours which takes into account the semi-infinite character of the solid. We refer to Ref. 23 for the results and a detailed discussion on this topic.

V. CONCLUSIONS

We have presented a method to investigate infinite non-periodic systems in the framework of the GWA. Calculations can be performed in finite regions, without introducing nonphysical boundary conditions, such as confining barriers (the slab approach) or a 3D fictitious periodicity (the supercell one). In such systems (e.g., a solid with a surface) densities of states are continuous, and while really discrete states may exist inside gaps, other ones become resonances when they do overlap in energy with a continuum band. The proposed method is particularly suitable for the description of these systems. In fact on the one side the embedding approach, which allows for calculating a truly continuous density of states, includes automatically the hybridization between bulk and surface states. On the other many-body effects, whose treatment is needed for excited states or image potential ones, are accounted for at the GWA level.

On the contrary a DFT slab calculation of such systems (e.g., in the LDA or GGA) is only able to work out a spectral weight constituted by delta functions, one for

each discrete eigenstate, while the real structure of the spectrum may be in general more complicate as just outlined. The GWA correction cannot amend by itself this result, but only determine a broadening of quasi-particle states (plus eventually minor additional structures) due to many-body correlations. This broadening, which can be evaluated in first approximation by taking the average value of the self-energy over the DFT state, may be much smaller than that due to hybridization effects, as it is the case for IPI resonances.

In this paper we have also extensively investigated semi-infinite jellium by our approach. We have illustrated the bulk-to-vacuum transition of the many-body electron gas properties. By comparing the LDA and GWA density of states, this method has been able to identify an image potential surface resonance of large width.²³ Extension of this approach to semi-infinite realistic surfaces could bring a wealth of accurate data on the spectral properties of surfaces and adsorbates, especially regarding the excited states.

Acknowledgments

We would like to thank M. I. Trioni and G. Onida for useful discussions. This work was supported by the Italian MIUR through Grant No. 2001021128.

APPENDIX: ANALYTIC CONTINUATION OF FREQUENCY INTEGRALS.

The presence of non-analyticities close to the contour of the frequency integration renders it difficult to integrate expressions containing the Green function G and the effective potential W numerically, as for the polarization or the self-energy.

Consider the integral defining the polarization P in Eq. (8) first. The Green function has poles (or cuts) just below the real ω axis for $\omega > \mu$ and above for $\omega < \mu$. Therefore, if z is a pole or a point in the cut, $\text{sgn}(\mu - \Re z) = \text{sgn}(\Im z)$. Note that the factor $e^{i\omega'\eta}$ implies that only the residues related to occupied states ($\omega < \mu$) are summed up. To avoid the just mentioned numerical difficulty, one can define the analytic continuation of P to complex frequencies as the sum over the same residues, now evaluated at a complex frequency.²⁴ It is easy to show that for purely imaginary frequencies this corresponds to rotate the integration contour to the complex frequency axis $\mu + iu'$ (u, u' real). In the GWA the continued polarization [Eq. (8)] is:

$$P_0(iu) = -2i \int_{\mu-i\infty}^{\mu+i\infty} d\omega' G_0(\omega' + iu) G_0(\omega'). \quad (A.1)$$

On the same footing, also the self-energy [Eq. (7)] can be continued to complex frequencies. If $\omega = \mu + iu$, the

following relation holds:

$$\Sigma_{XC}(\mu + iu) = i \int_{-i\infty}^{i\infty} d\omega' G_0(\omega' + \mu + iu) W_0(\omega') \quad (\text{A.2})$$

where the analytic continuation of $W_0(\omega' = iu')$ is evaluated by inserting $P_0(iu)$ into Dyson's equation. Note that the Lehmann representation of P_0 implies that a pole z of W_0 has $\text{sgn}(\Im z) = -\text{sgn}(\Re z)$.

The self-energy resulting from Eq. (A.2) will be known on the complex line $\omega = \mu + iu$. This is useful for the evaluation of integral properties (e.g., the total energy), but for spectral properties the Green function (and hence the self-energy) has to be known at real frequencies. To this end, one can fit Σ_{XC} on the complex axis with a simple analytic expression, to be continued to the real axis.²⁵ The multi-pole expansion is perhaps the more common one:

$$\Sigma_{XC}(\omega) = a_0 + \sum_{j=1}^N \frac{b_j}{\omega - c_j}. \quad (\text{A.3})$$

A small number of poles ($N = 2 \sim 4$) normally provides a good fit.

Finally we recall a useful result to rotate the integration path in frequency space. Consider the two integrals, where ω , a and b are real:

$$F_1(\omega) = \int_{-\infty}^{+\infty} d\omega' \frac{1}{(\omega' - z_1)(\omega + \omega' - z_2)} \\ = i\pi \frac{\text{sgn}(\Im z_1) - \text{sgn}(\Im z_2)}{\omega - z_2 + z_1} \quad (\text{A.4})$$

$$F_2(\omega) = \int_{a-i\infty}^{a+i\infty} d\omega' \frac{1}{(\omega' - z_1)(b + i\omega + \omega' - z_2)} \\ = i\pi \frac{\text{sgn}(a - \Re z_1) - \text{sgn}(a + b - \Re z_2)}{b + i\omega - z_2 + z_1} \quad (\text{A.5})$$

The two numerators are equal if $\text{sgn}(\Im z_1) = \text{sgn}(a - \Re z_1)$ and $\text{sgn}(\Im z_2) = \text{sgn}(a + b - \Re z_2)$. In this case: $F_2(\omega) = F_1(b + i\omega)$, i.e., F_2 is the analytic continuation of F_1 to complex frequencies $b + i\omega$. Notice that, to be analytic, the continuation has to be performed *after* the integration.

If both z_1 and z_2 are poles of the time-ordered Green function [as for the polarization, Eq. (8)], it follows from the Lehmann representation that the condition is met for $a = \mu$ and $b = 0$. If z_1 is a pole of the effective interaction and z_2 is a pole of the time-ordered Green function [as for the self-energy, Eq. (7)], the condition is met for $a = 0$, $b = \mu$.

* Present address: SISSA/ISAS, via Beirut 4, I-34014 Trieste; Electronic address: fratesi@sisssa.it
 † Electronic address: gianpaolo.brivio@mater.unimib.it
 ‡ Electronic address: luca.molinari@mi.infn.it
¹ A. E. Mattsson and W. Kohn, *J. Chem. Phys.* **115**, 3441 (2001).
² A. G. Eguiluz, M. Heinrichsmeier, A. Fleszar, and W. Hanke, *Phys. Rev. Lett.* **68**, 1359 (1992).
³ L. Hedin, *Phys. Rev.* **139**, A796 (1965).
⁴ W. G. Aulburg, L. Jönsson, and J. W. Wilkins, *Solid State Physics*, edited by H. Ehrenreich and F. Spaepen (Academic, New York, 2000), vol. 54.
⁵ F. Aryasetiawan and O. Gunnarsson, *Rep. Progr. Phys.* **61**, 237 (1998).
⁶ G. Onida, L. Reining, and A. Rubio, *Rev. Mod. Phys.* **74**, 601 (2002).
⁷ G. P. Brivio and M. I. Trioni, *Rev. Mod. Phys.* **71**, 231 (1999).
⁸ S. Brodersen and W. Schattke, *Phys. Rev. B* **66**, 153303 (2002).
⁹ W. Kohn, *Phys. Rev. Lett.* **76**, 3168 (1996).
¹⁰ W. Kohn and A. E. Mattsson, *Phys. Rev. Lett.* **81**, 3487 (1998).
¹¹ P. G. González and R. W. Godby, *Phys. Rev. Lett.* **88**,

054606 (2002).
¹² A. Fetter and J. D. Walecka, *Quantum Theory of Many Particle Systems* (Mac Graw Hill, New York, 1971).
¹³ A. Schindlmayr, cond-mat/0206510 (unpublished).
¹⁴ B. Holm and U. von Barth, *Phys. Rev. B* **57**, 2108 (1998).
¹⁵ J. E. Inglesfield, *J. Phys. C: Solid State Phys.* **14**, 3795 (1981).
¹⁶ J. E. Inglesfield and G. A. Benesh, *Phys. Rev. B* **37**, 6682 (1988).
¹⁷ M. I. Trioni, G. P. Brivio, S. Crampin, and J. E. Inglesfield, *Phys. Rev. B* **53**, 8052 (1996).
¹⁸ C. Menchini, M. I. Trioni, and G. P. Brivio, *Phys. Rev. B* **67**, 035408 (2003).
¹⁹ J. F. Dobson, *Density Functional Theory*, NATO ASI Series B: Physics, edited by E. K. U. Gross and R. M. Dreizler (Plenum, New York, 1995), vol. 337, p. 393.
²⁰ P. Sánchez-Friera and R. W. Godby, *Phys. Rev. Lett.* **85**, 5611 (2000).
²¹ R. Matzdorf, *Surf. Sci. Repts.* **30**, 153 (1998).
²² S. Schintke, S. Messerli, M. Pivetta, F. Patthey, L. Libioulle, M. Stengel, A. D. Vita, and W.-D. Schneider, *Phys. Rev. Lett.* **87**, 276801 (2001).
²³ G. Fratesi, G. P. Brivio, P. Rinke, and R. W. Godby (unpublished).

²⁴ R. W. Godby, M. Schlüter, and L. J. Sham, Phys. Rev. B **37**, 10159 (1988).

²⁵ M. M. Rieger, L. Steinbeck, I. D. White, H. N. Rojas, and

R. W. Godby, Comp. Phys. Comm. **117**, 211 (1999).